High-performance polymer-based regenerative elastocaloric cooler

Gael Sebald, Giulia Lombardi, Gildas Coativy, Jacques Jay, L Lebrun, Atsuki Komiya

▶ **To cite this version:**

Gael Sebald, Giulia Lombardi, Gildas Coativy, Jacques Jay, L Lebrun, et al.. High-performance polymer-based regenerative elastocaloric cooler. Applied Thermal Engineering, 2023, 223, pp.120016. 10.1016/j.applthermaleng.2023.120016 . hal-04083991

HAL Id: hal-04083991
https://hal.science/hal-04083991

Submitted on 28 Apr 2023

HAL is a multi-disciplinary open access archive for the deposit and dissemination of scientific research documents, whether they are published or not. The documents may come from teaching and research institutions in France or abroad, or from public or private research centers.

L'archive ouverte pluridisciplinaire **HAL**, est destinée au dépôt et à la diffusion de documents scientifiques de niveau recherche, publiés ou non, émanant des établissements d'enseignement et de recherche français ou étrangers, des laboratoires publics ou privés.

Revised Manuscript (clean version) Click here to view linked References

High-performance polymer-based regenerative elastocaloric cooler

Gael Sebald[a], Giulia Lombardi[a,b], Gildas Coativy[c], Jacques Jay[d], Laurent Lebrun[c], Atsuki Komiya[a,b]

[a] *ELyTMaX IRL3757, CNRS, Univ. Lyon, INSA Lyon, Centrale Lyon, Université Claude Bernard Lyon 1, Tohoku University, 980 8577, Sendai, Japan*

[b] *Institute of Fluid Science, Tohoku University, 980 8577, Sendai, Japan*

[c] *Univ. Lyon, INSA Lyon, LGEF EA682, F69621, Villeurbanne, France*

[d] *Univ. Lyon, CNRS, CETHIL, INSA Lyon, F69621, Villeurbanne, France*

Corresponding authors: Gael Sebald (gael.sebald@insa-lyon.fr), Giulia Lombardi (giulia.lombardi.a1@toholu.ac.jp)

Abstract

Alternative methods of refrigeration are critical for performance optimization and environmental sustainability. Prototype systems using caloric materials have shown the advantages of a high coefficient of performance (COP) and low global warming potential. Elastocaloric elastomers can meet ongoing needs, but their implementation in functional heat pumps or coolers remains challenging due to their requirement for a large deformation and low thermal conductivity. Moreover, a scalable design is required to achieve high cooling power. As a leap forward for the use of polymers in larger scale caloric devices, we developed experimental elastocaloric polymer coolers with two different geometries using natural rubber tubes. We confirmed that a suitable geometry partially compensated for the low thermal conductivity and led to performances comparable to those of other caloric devices. Several operating conditions were tested to determine the optimal temperature span, cooling power, and COP for both device geometries. Under a specific operating condition, one of the prototypes exhibited a maximum temperature span >8 K, a maximum COP of 6, and an output cooling power of 1.5 W; this power outperforms other prototypes based on polymers or ceramics. The parallelization of rubber tubes will facilitate realistic elastocaloric polymer coolers on a larger scale.

Keywords: Solid-state cooling, caloric materials, active regeneration, elastocaloric, natural rubber

Symbol	***Property***	***Unit***
COP	coefficient of performance	[-]
NR	natural rubber	
λ	elongation	[-]
λ_{max}	maximum elongation	
ABS	acrylonitrile butadiene styrene	
d_{ext}	external diameter	[m]
d_{int}	internal diameter	[m]
ΔT_{ad}	adiabatic temperature change	[K]
ΔT_{pp}	peak-to-peak adiabatic temperature change	[K]
ΔT_{span}	device temperature span	[K]

COPmat	material coefficient of performance	[-]
Whyst	intrinsic hysteresis loss	[J m^{-3}]
Wm	mechanical losses	[J m^{-3}]
Wh	hydraulic losses	[W]
$\dot{Q}_C$	cooling power	[W]
V*	ratio between the volume of moving fluid and the total fluid volume inside regenerator's tubes	[-]
V_{tot}	total volume of the reservoir	[l]
V_{reg}	volume of regenerator	[l]
$\dot{V}_r$	flow rate	[l s^{-1}]
T_{top}	temperature of the top reservoir	[°C]
T_{bottom}	temperature of the bottom reservoir	[°C]
T_{amb}	ambient temperature	[°C]
f	frequency	[s^{-1}]
ρ	natural rubber density	[kg m^{-3}]
ρ_f	fluid density	[kg m^{-3}]
p	static pressure	[N m^{-2}]
G	constant of gravity	[N kg^{-2} m^{-2}]
Cp	specific heat capacity	[J Kg^{-1} K^{-1}]
N	Network chain density	[mol cm^{-3}]
k	Boltzmann constant	[m^2 kg s^{-2} K^{-1}]
δ	harmonic thermal boundary layer thickness	[m]
K	thermal conductivity	[W m^{-1} K^{-1}]
ω	angular frequency	[rad s^{-1}]
U	voltage	[V]
α	hydraulic loss coefficient	[-]
R	resistance	[Ω]
F	measured force	[N]
v	actuator speed	[m s^{-1}]
h_{eff}	effective heat exchange coefficient	[W m^{-2} K^{-1}]
h	heat transfer coefficient	[W m^{-2} K^{-1}]
Bi	Biot number	[-]
Re	Reynolds number	[-]
Nu	Nusselt number	[-]
a_0	Geometric factor	[-]
$R_{TH\_conduction}$	Conduction thermal resistance	[K W^{-1}]
$R_{TH\_convection}$	Convection thermal resistance	[K W^{-1}]

1. Introduction

Over the last three decades, energy consumption for ambient cooling has more than tripled, now accounting for almost 20% of the electricity consumed in the building sector [1]. Implementing not only more efficient but also environmentally friendly technologies could help ambient cooling reach the target of net zero emissions by 2050. Currently, vapor compression refrigeration remains the most widespread technology, with its biggest drawback being the use of high-global-warming potential refrigerant gases that are released in the atmosphere.

Environmentally friendly alternatives include CO_2 heat pump systems, CO_2 being a natural, non-toxic, and non-flammable refrigerant [2]. However, these systems face significant challenges, for instance, the low critical point of CO_2 (7.38 MPa and 31.1 °C [3]) and the high operating pressure required to induce the liquefaction of CO_2 (8 to 11 MPa [4]), which impact the efficiency of the pumping system and pose additional challenges for the optimization of the Coefficient of Performance (COP) [5].

Another course of action toward the replacement of refrigerant gases is represented by

solid-state cooling systems based on caloric materials. Because of their low global warming potentials, systems based on caloric materials could ameliorate the current tradeoff between the performance, toxicity, and environmental issues of refrigerant gases [6,7].

Caloric materials exhibit large entropy variations when subjected to an electric field, a magnetic field, or mechanical stress or pressure. Such materials may be useful in heat engines and experimental proofs-of-concept for alternative refrigeration technologies [8]. When the appropriate parameter (e.g., mechanical stress) is applied or removed, such materials exhibit self-heating or self-cooling, leading to time variations of their temperature. In a cooling device, a system is required to transform these time variations of the caloric material temperature into a permanent spatial gradient.

One solution consists of moving the caloric material into contact with a cold or hot heat exchanger, leading to so-called single-stage systems [9]. An alternative way is to use a heat transfer fluid transporting heat bidirectionally to and from the active material, leading to the so-called active regenerative systems. An active regenerative process is thus achieved by applying and removing an external field (e.g., mechanical stress) to the caloric material using mechanical power and synchronizing the caloric response with the reciprocating circulation of the heat transfer fluid. This will induce both the caloric material and the heat transfer fluid to move cyclically. This process solves the time-to-space conversion issue, but also enables the temperature span of the system to be higher than the adiabatic temperature change of the active material [10–12]. Active caloric regeneration has been extensively investigated for magnetocaloric devices [11–14]. The latest significant development was achieved with a 15 kW magnetocaloric proof-of-concept unit, developed by Lionte et al., with a temperature san of 20 K [15]. Active regeneration has later been applied for other domains of caloric materials as well. Electrocaloric ceramics were used for several works [10,16]. For instance, 13 K of temperature span and a cooling power of 1.22 W were obtained by Torello *et al*. [10]. Elastocaloric devices based on shape-memory also reached promising results [17–21]: the device developed by Tusek *et al.* exhibited a temperature span of 15.3 K with a corresponding specific power of 800 Wkg^{-1} [17] while 14 K with a corresponding specific power of 4400 Wkg^{-1} were reached with a device developed by Ahcin et al. [21].

Despite the latest considerate improvements, except for magnetocaloric devices, refrigeration based on the regenerative process is still at laboratory scale with cooling power not exceeding a few W. In the long term, however, regenerative cooling systems may penetrate the market of cooling devices as a replacement of the vapor-compression technology if a strong research effort is done. Long term research objectives focus on the improvement of the device (scaling up and realistic use conditions) and material performances (not only ΔT_{ad} , but also fatigue life and thermal properties) as well as proposing alternative caloric materials (ensuring the availability of the material for massive implementation). In this regard, polymers find considerable advantages, despite their application in regenerative cooling devices have not been investigated yet.

Compared with other caloric materials, polymers exhibit a low COP footprint for their fabrication and are low cost. The elastocaloric effect in polymers can be qualified as a change in temperature on the material when subjected to mechanical solicitations. Recent work of elastocaloric polymers includes membrane inflation, torsional deformation, and electrocaloric polymers [22–24]. These previous works on polymers introduced the high potential of these materials for cooling purposes but did not provide a solution for large-scale development, because a single material sample of a few tens of milligram was tested. The actuation of the sample required bulky systems, leaving the question of the feasibility of upscaling the devices unsolved. Realistic cooling devices, with a cooling power ranging from 10 W to 10 kW, would

require hundreds of grams or kilograms of active materials, the assembly of which is a challenge in itself, as it requires the structure to remain highly compact due to heat loss issues [15].

For some elastomers, such as natural rubber or some polyurethanes, the origin of the elastocaloric effect relies on the strain induced crystallizations (SIC) and entropic elasticity [28,29]. The former refers to the partial transformation of the amorphous polymer chains into a crystalline state when a certain deformation is applied, and the latter is based on the decrease of entropy of polymer chains under stretching. This causes the entropy of the material to decrease so that the material exchanges heat with the surroundings. The cooling effect seen on these materials require a total or a partial reversibility of these two phenomena. Therefore, only a large deformation leads to considerable elastocaloric activity that is attributable to strain-induced crystallization and entropic elasticity. The values of the applied deformation (up to 600%) thus make scalable polymer-based cooling applications a challenge. Nevertheless, pre-elongated natural rubber driven by uniaxial strain results in moderate activity [25] yet excellent fatigue life [26,27] (>100k cycles), similar to the best-performing elastocaloric materials [28].

Moreover, polymers possess low thermal conductivities (1/5th of those of ceramics and 1/100th of those of metals), which limits the exchange between the heat transfer fluid and rubber but also favors a thermal gradient inside the material in the longitudinal direction.

To address the potential issue of a low thermal conductivity, previous theoretical work [29] indicated that the geometry might accommodate the thermal properties (thermal conductivity and heat capacity) when the material's thickness is similar to or smaller than that of the harmonic thermal boundary layer. The thermal properties can also be explained by the direct proportionality of the thickness of the material to its thermal resistance: the thicker the material is, the higher the thermal resistance becomes. The previously mentioned principles have been validated only partially on a single natural rubber tube sample of a few milligrams. Thus, a full cooling-rubber-based regenerative device needed to be developed, with cooling performance evaluation. In this work, two active all-polymer regenerative systems using natural rubber tubes are presented. Experimental evidence of the impact of the geometry is given, based on both the temperature span and the cooling power determination. The novelty of this work lies in the application of active regenerative cooling combined with the use of numerous parallel, highly stretchable rubber tubes. We demonstrate the competitiveness of natural rubber for scalable regenerative cooling systems based on the performances achieved by the devices proposed in this work. We focused on the performance of the devices in terms of cooling capabilities only, but the devices can work as heat pumps as well (generating heat instead of removing it). The cooling power, COP, and temperature span were comparable to those of other caloric-material-based heat pumps and coolers, whereas the applied tensile stress was hundreds of times less than those of Ni-Ti alloys [17].

2. Elastocaloric material properties

Natural rubber (NR) tubes were selected as an elastocaloric material for the fabrication of the cooling devices, due to the relatively low values of applied tensile force compared to those of other elastocaloric materials [17]. NR tubes were purchased from Omega Engineering (Norwalk, Connecticut, USA). Two different tube geometries were used to fabricate the devices: for NR tubes of the first device (Device #1), the internal and external tube diameters were 3.18 and 4.76 mm, respectively (commercial reference OMEGAFLEX Natural Latex TYGR-31618-50). For the NR tubes of the second device (Device #2), the internal and external diameters

were 1.59 and 3.18 mm, respectively (commercial reference TYGR-18116-100). Table 1 shows the nominal properties from the supplier's datasheet.

Hardness, Shore A	35±5
Specific gravity	0.95
Tensile strength	24.1 MPa
Elongation at break	750%

Table 1: Properties of the natural rubber tubes used in this study as provided by the supplier (https://www.omega.co.uk/pptst/TYGR.html)

To investigate the elastocaloric properties of the NR tubes, a combination of a mechanical tensile test bench with an infrared camera was used. The test bench consisted of a single-axis robot RSDG212 (MISUMI Corporation, Tokyo, Japan) with an analog force sensor XFTC300–200N (TE Connectivity, Schaffhausen, Switzerland). A laser optical displacement sensor ILD1420–200 (Micro-Epsilon, Saint Germain en Laye, France) was used to measure the displacement and the corresponding elongation $\lambda = {}^{l(t)}/_{l_0}$, defined as the ratio between the length l at time t and the initial length l_0. A thermal camera, Optris PI450 (Optris, Berlin, Germany), was used to measure the surface temperature of the rubber tube.

The sample, consisting of a single rubber tube, was fixed at both ends to parts of acrylonitrile butadiene styrene (ABS) mounted onto the displacement actuator. To determine the adiabatic temperature variation, the rubber tube was stretched from the nonelongated state up to different maximum elongations (i.e., λ_{max} = 3.5, 4, 4.5, 5, 5.5, and 6) at 320 mm–s^{-1}, leading to an abrupt increase in the surface temperature due to the strain-induced crystallization and the orientation of the chains toward the strain direction (entropic elasticity) [30,31]. The stretched position was maintained for 150 s, when thermal equilibrium was reached. After this time, the sample was retracted at the same speed until the point at which $\lambda = 1$, leading to an abrupt decrease in the surface temperature due to the melting of the crystals and the chain disorientation; the position was maintained until thermal equilibrium was reached again. All the samples were tested at ambient temperature (*i.e.* 20°C).

A maximum adiabatic temperature ΔT_{ad} of 13.8 K and a maximum stress of 2 MPa was recorded for the NR of Device #1 at λ = 6, corresponding to a hysteresis of 4.1 MJ m^{-3}. As per the NR of Device #2, a maximum adiabatic temperature ΔT_{ad} of 10.8 K and a maximum stress of 1.5 MPa were recorded at λ = 6, corresponding to a hysteresis of 3.7 MJ·m^{-3}. These results are consistent with those of the literature on NR [25,32,33]**.**

The intrinsic average power loss coming from mechanical hysteresis W_{hyst} of the rubber tubes was determined by the average over one period of the mechanical power:

$$\dot{W}_{hyst} = f \int_0^{1/f} F(t)v(t)dt \quad (1)$$

The material coefficient of performance COP_{MAT}, defined as the potential absorbed heat when retracting the material divided by the hysteresis loss W_{hyst} [34], was calculated as:

$$COP_{MAT} = {}^{\rho C_p \Delta T_{ad}}/_{W_{hyst}} \quad (2)$$

where ρ and C_p are the density (950 kg·m^{-3}) and the specific heat capacity (1800 J·kg^{-1}·K^{-1})

of the NR, respectively, and assumed to remain constant near room temperature.

We found a maximum value of COP_{MAT} of 7.3 for the NR tube of Device #1. Based on the NR of Device #2, the maximum COP_{MAT} was 8.2.

The network chain density N was then estimated from stress–strain curves at low elongation. For low elongation levels, the elasticity can be assumed to be driven as follows [35,36]:

$$\sigma = NkT(\lambda - \lambda^{-2}) \quad (3)$$

where σ is the stress, T is the working temperature, λ is the elongation at low levels, and k is the Boltzmann constant. A value of 1.25×10^{-4} mol· cm^{-3} was found for the NR tube used for Device #2 while a value of 1.6×10^{-4} mol· cm^{-3} was found for the NR tube used for Device #1. These values are consistent with other weakly crosslinked NRs [36].

Cyclic elastocaloric properties were studied by imposing trapezoidal cyclic elongations consisting of a 4 s strain application, a 1 s pause, 4 s of strain release and a 1 s pause at 0.1 Hz with a bias pre-elongation. Three different cyclic elongations were applied to the sample: between $\lambda = 3$ and $\lambda = 5$, between $\lambda = 3.5$ and $\lambda = 5.5$, and finally between $\lambda = 4$ and $\lambda = 6$. Fig. 1 shows the resulting temperature variation as a function of time (Fig. 1(A)) along with the stress–strain curves (Fig. 1(B)). The results refer to the NR tube used in Device #2 for cyclic elongation between $\lambda = 3.5$ and $\lambda = 5.5$. For this case, the peak-to-peak temperature variation ΔT_{pp} stabilized after approximately 20 cycles, reaching 3.5 K and corresponding to the adiabatic temperature variation ΔT_{ad}. For the other types of elongation, similar values of the peak-to-peak temperatures ΔT_{pp} were obtained, with a difference of ± 9% between each tested elongation. The mechanical losses over the last two cycles of each cyclic test were found to be small (0.27 MJ·m^{-3} ± 0.08 MJ·m^{-3} for each elongation), leading to a COP_{MAT} value of 22 ± 5 for each elongation. Higher COP_{MAT} values were obtained for the smallest elongation range, due mainly to a reduction of the hysteresis in the rubber tube under the lower value of an applied tensile force. This trend justifies the interest in cycling elongations between $\lambda = 3.5$ and $\lambda = 5.5$, as it represents an appropriate compromise between the temperature variations and the mechanical losses.

Similar results were obtained for the NR tube used for Device #1: a peak-to-peak temperature ΔT_{pp} of 3.7 K was obtained for elongations between $\lambda = 3.5$ and $\lambda = 5.5$, with a difference of ± 0.3K between each tested elongation condition. The mechanical losses were measured to be 0.29 MJ·m^{-3} ± 0.07 MJ·m^{-3} for each elongation, leading to a COP_{MAT} value of 22 ± 3.5. Again, higher values of COP_{MAT} were recorded for smaller elongations, which explains the interest in employing cycling elongations between $\lambda = 3.5$ and $\lambda = 5.5$ for the NR tube of Device #1 as well.

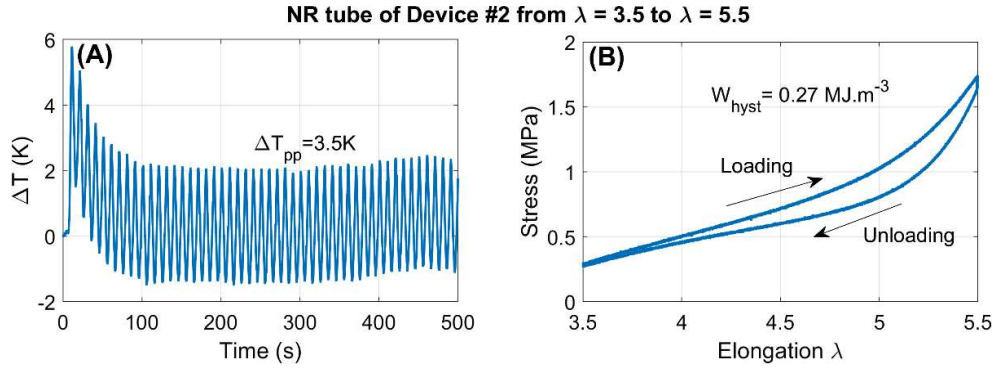

Fig. 1. Cyclic elastocaloric properties for the natural rubber (NR) tube of Device #2. (A) ΔT as a function of time for cyclic elongations at 0.1 Hz between $\lambda = 3.5$ and $\lambda = 5.5$. **(B)** Stress–elongation curve as a function of time for cyclic elongations at 0.1 Hz between $\lambda = 3.5$ and $\lambda = 5.5$.

3. Fabrication and design of cooling devices

Prior to fabricating the regenerators, a rubber tube with an initial length of 1.5 m was stretched to an elongation of 6 (i.e., 9 m) and maintained stretched at this length for 3 min. The tube was then released back to its initial length. There was negligible remnant strain (<1%). The tube was cut into shorter tubes of equal length (50 mm). The tube was mounted into a printed ABS plate with holes to facilitate inward tube passage at both ends for approximately 1 cm. The ends of the tubes were then mechanically fixed onto each plate, and the tubes were stretched until an elongation of 4. Epoxy resin was poured onto the ABS plate on both ends to freeze the outer position of the rubber tubes and to leave the inner part empty for future water flow between the tubes and the reservoirs. The tubes were then stretched until an elongation of 6, and a second layer of epoxy was poured onto both ends, to ensure that both elongations are mechanically stable. When stretched, the rubber tubes changed from their initial outer diameter to the final diameter, which was approximately half of the initial diameter. Near the fixing location on the ABS plate, the tube was observed to have a conical shape and was fully embedded into the epoxy resin. The epoxy sealing solved the challenge of achieving a proper grip of the rubber tubes, leading to an all-polymeric cooling device.

Fig. 2 shows pictures of the final mounting of the tubes for Device #1 and Device #2. The tube diameter from the boundary of the epoxy was already at its final value, ensuring the homogeneity of the elastocaloric effect along the length of the tube. Supplementary Table S1 and Table S2 provide details of the geometries of the regenerators.

The device consisted of numerous parallel NR tubes, actuated along their axes by pre-elongation to solve the otherwise limiting issue of the large strain of NR), with a heat transfer fluid (water) flowing inside the tubes. We fabricated two configurations, Device #1 (19 tubes; the inner diameter of each tube was 3.2 mm) and Device #2 (55 tubes; the inner diameter of each tube was 1.6 mm), to investigate the impact of the fluid channel diameter on the regenerator performance. The wall thicknesses of the fully elongated tubes were approximately 300–450 μm for both configurations.

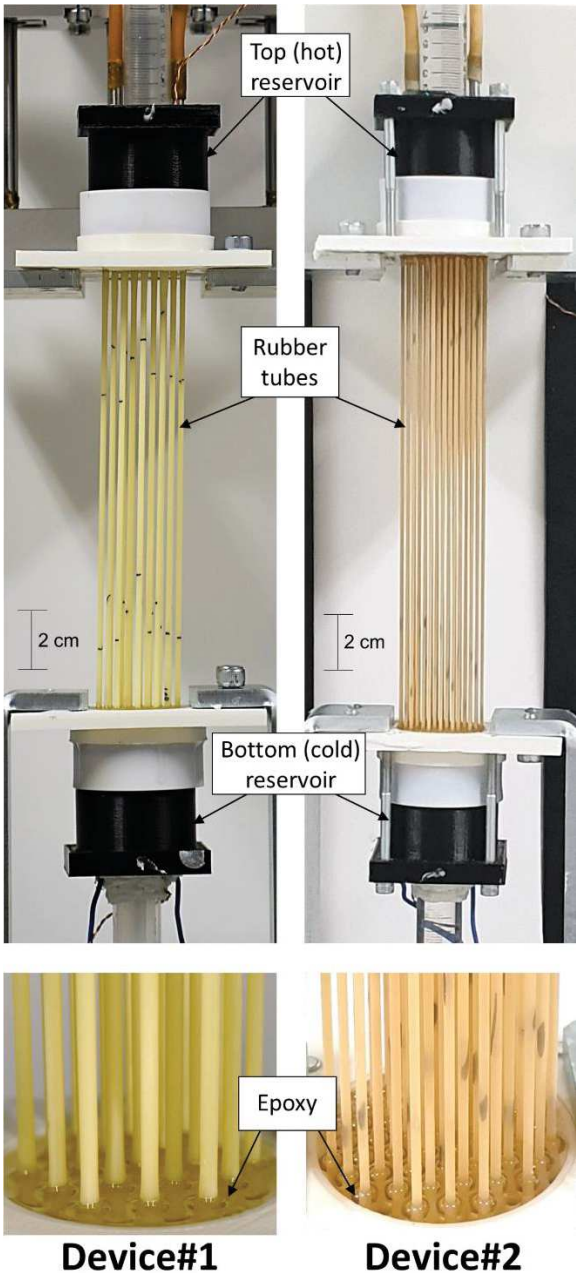

Fig. 2. Fabricated devices. Device #1 consists of 19 tubes of initial external diameter 4.76 mm and Device #2 consists of 55 tubes of initial diameter 3.18 mm. The black areas on the rubber tubes are marks made before the regenerator fabrication. Two marks spaced by 20 mm were first drawn. After stretching the regenerator, the measurement of the distance between the marks facilitated verification of the actual elongation.

4. Experimental method

4.1. Experimental setup

The regenerators were mounted onto a testing experimental setup, including an actuator for regenerator stretching (MISUMI RSDG306, Tokyo, Japan) and a piston pump with its actuator (MISUMI RSD112, Tokyo, Japan). Control of both actuators was achieved with the MATLAB Instrument Control Toolbox to ensure synchronization of both motions. The motors of the actuators were air-cooled by fans to avoid heating the actuator shaft by thermal conduction. The displacements of both actuators were measured with laser displacement sensors (Panasonic

displacement sensors HG-C1400 and HG-C1100-P, Kadoma, Japan – uncertainty of ±10 μm).

Small reservoirs (6.4 mL each) were placed at both ends of the regenerator. Both the bottom and up reservoirs were thermally insulated with polyurethane foam. The bottom reservoir was incorporated a 96 mΩ heating resistor for adding a heat source to the bottom (cold) reservoir. An intentionally small value was chosen such that the voltage on the resistance remained below 1 V up to 10 W of heating power to avoid electrolysis of the water. Short-length conical shape diffusors were added inside each reservoir to homogenize the fluid flow and limit the dead volumes [37]. The top reservoir was left open to ensure that the pressure remained constant inside the regenerator.

At the bottom of the entire system, a force sensor (Vishay Tedea Huntleigh load cell #615, Malvern, PA, USA – uncertainty of ±0.05 %) was mounted. The total static force of the regenerator, the actuator for the fluid motion, and the reservoir was 41.6 N, which was subtracted from the measurement. This static force in all cases had no influence on the determination of the mechanical power of the rubber that was obtained by averaging the periodic instantaneous mechanical power over one period.

To characterize the elastocaloric effect, the surface temperature of the rubber tubes constituting the regenerators was measured with an infrared camera (Optris Xi400, Berlin, Germany). To test the elastocaloric refrigeration device, the temperature was measured at several locations using thermocouples (uncertainty of ±0.05°C): inside the hot heat exchanger, inside the cold heat exchanger, at the inlet and outlet of the circulation of the fluid of the hot heat exchanger, and outside the system as a measure of the ambient temperature. All thermocouples were calibrated with a temperature-controlled water bath to subtract the static error of each thermocouple.

All measured quantities were collected with a Digital Acquisition module (Dewesoft Krypton, Trbovlje, Slovenia). Fig. 3(B) shows a photograph of the experimental setup.

The measurement uncertainties were evaluated based on the specifications of the experimental equipment. The measurement error corresponding to the evaluation of the cooling power was set to ±0.05% whereas the temperature error was set to ±0.2 °C. Despite the absolute accuracy of the IR camera used during the experiments is declared as ±1°C, its relative accuracy has been demonstrated to actually be higher, with typical noise level values of ±0.2 °C [38].

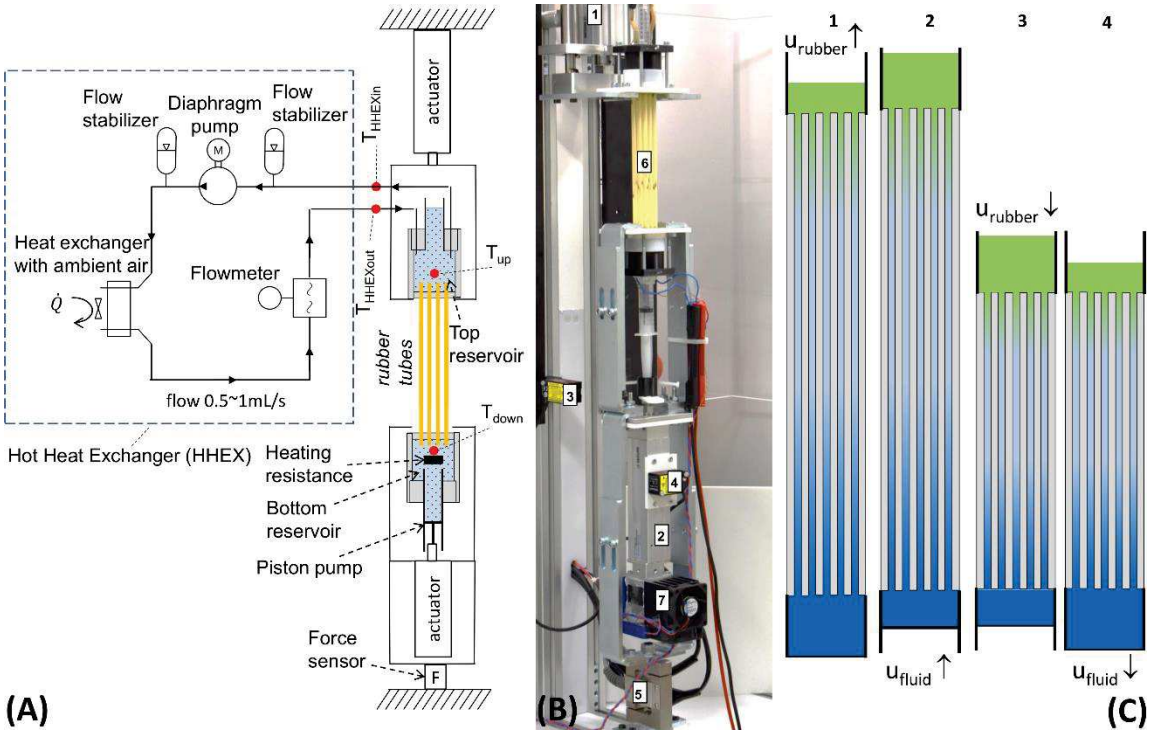

Fig. 3. Experimental system. (A) Experimental setup. **(B)** Main components of the experimental setup: (1) main actuator, (2) piston pump actuator, (3) optical displacement sensor for the main actuator, (4) optical displacement sensor for the pump actuator, (5) force sensor, (6) rubber tubes, and (7) fans for cooling the actuator motor. For the sake of clarity the thermal insulation around both reservoirs were removed. **(C)** Cooling device operation principle. Step 1: rubber tubes are stretched to an elongation of 5.5. Step 2: water is moving up inside the regenerator from the bottom (cold) reservoir. Step 3: rubber tubes are returned to an elongation of 3.5. Step 4: water is moved down from the top reservoir.

4.2. Operation of the cooling devices

There is a few evidence only concerning the dependence of the elastocaloric effect of natural rubber under different operating temperatures. Under large elongation, from previous work, the elastocaloric effect of natural rubber was found to be decreasing from 9K to 7.5K for ambient temperature ranging from 5°C up to 27°C, with peak activity of 12K around 10°C [39], indicating that natural rubber is especially well suited for refrigeration from room temperature. It is also supported by other studies on the influence of temperature on strain induced crystallization of natural rubber: at low temperature, the elastocaloric effect should be reduced, because the crystals formed during stretching cannot melt while at high temperature crystallization cannot occur [40].

At first, both regenerators were tested without heat transfer fluid to determine the elastocaloric temperature change under quasi-adiabatic condition, assuming that the natural convection of the air in contact with the rubber tubes is negligible at his time scale. Both devices were tested at ambient temperature (*i.e.* 25°). During operation, we stretched the tubes cyclically between elongations of approximately 3.5 to approximately 5.5 at 0.1 Hz. Supplementary Movie S1 shows an example of characterization on Device #2 after 4000 cycles. After 10,000 cycles, an adiabatic temperature of 3.3 K was observed for Device #1. For Device #2, an adiabatic temperature of 3.6 K was recorded after 10,000 cycles when subjected to the same conditions of Device #1 (elongations of approximately 3.5 to 5.5 at 0.1

Hz).

Subsequently, the regenerators were filled with the heat transfer fluid (water). The water volume was enough to completely fill in the tubes and the two reservoirs, so that during functioning all the system remain filled with water. A dedicated hydraulic circuit was designed, the schematic of which is given in Fig. 3(A). The inner diameter of the tubes when stretched was determined by the change in the regenerator fluid volume during stretching. The regenerator was initially filled with the fluid, and gradually stretched until a maximum elongation of 6. For each elongation, the relative volume change was read at the top of the upper reservoir. Given the initial diameter of the tubes, and assuming that the rubber material volume was almost constant (Poisson ratio ~0.5), the inner and outer diameters were determined for the tested elongations. For Device #1, the inner diameter ranged from 1.45 mm (elongation of 6) to 1.78 mm (elongation of 4). For Device #2, the inner diameter ranged from 0.77 mm (elongation of 6) to 0.94 mm (elongation of 4).

The tube wall thickness of the rubber tubes ranged from 300 to 450 μm for both devices between an elongation from 4 to 6. The thickness δ of the harmonic thermal boundary layer (typically the distance from the edge of the rubber for which temperature variation amplitude is 37% of that of the edge with Neumann boundary condition) in the rubber tube is given by [29,41]:

$$\delta = \sqrt{2K/\rho C_p \omega}, \quad (1)$$

where K, ρ, C_p, and ω are the thermal conductivity (0.18 $W \cdot m^{-1} \cdot K^{-1}$), density (950 $kg \cdot m^{-3}$), and specific heat capacity (1800 $J \cdot kg^{-1} \cdot K^{-1}$) of rubber and the angular frequency of the fluid motion (0.63 $rad \cdot s^{-1}$), respectively. Considering the operating conditions and the properties of NR, a thermal boundary layer thickness of 600 μm was determined, which was much larger than the wall thickness.

The principle of operation for the devices consisted of a four-step process (Fig. 3(C)):

1. First, the rubber tubes were strained until the elongation reached approximately 5.5 in the absence of fluid flow, which caused the rubber to heat up due to the elastocaloric effect;
2. Then, while the regenerator remained strained, fluid is pushed by the piston pump through the heated tubes from the cold reservoir to the hot reservoir, thus rejecting the heat to the surroundings;
3. The elongation was then reduced to 3.5, causing the temperature of the material to decrease due to the elastocaloric effect;
4. Finally, fluid flowed down from the hot to the cold reservoir to absorb the cooling load Q_c while the rubber tubes were kept unstrained.

This four-step process was repeated cyclically, causing the temperatures of both reservoirs to evolve over time. This measurement corresponded to thermally unloaded conditions, since no heating power was introduced into the system.

Therefore the system exhibited two distinct characteristic times. The first one was related to the heat exchange between the fluid and the rubber tubes, and linked to the wall thickness and fluid channel radius. Considering the small dimensions involved here, frequency ranging from 0.1 Hz to 0.2 Hz was considered to be low enough to achieve the heat exchange between the rubber tubes and the fluid. The second characteristic time corresponded to the time to move down or up the base line of the temperature and to stabilize it at a given temperature span. It is related to the total thermal mass of the system and a typical time constant of 500s was observed.

To estimate the cooling power of the regenerators, the same protocol reported previously [17] was used. We connected the top reservoir of the devices to a heat exchanger via a fluid circulation system to maintain the reservoir temperature close to the ambient temperature (in this process, the diaphragm pump is thus activated to stabilize the temperature of the top reservoir). The temperature of the upper reservoir remained constant, whereas the temperature of the lower reservoir decreased until reaching stabilization. After the temperature stabilized, we powered a heating resistance unit placed in the bottom (cold) reservoir by varying the value of the current. With the increase in the imposed power, the temperature span between the ambient temperature and the cold reservoir decreased linearly. The maximum power was obtained when the temperature of the cold reservoir reached ambient temperature. This measurement corresponded to thermally loaded conditions, because the heating power was introduced in the system though the resistor placed in the bottom reservoir.

4.3. Determination of cooling power and COP

The characterization of the refrigeration prototype included the measurement of the temperature span, which was directly obtained by the thermocouple. For the cooling power, the heating power of a resistor placed in the insulated bottom reservoir was measured. A constant voltage was applied to the heating resistor during the characterization.

The generated power was assumed to be close to the cooling power $\dot{Q}_C$ (in watts). In all cases, this assumption underestimated the cooling power of the cooling device, as some of the pumped heat translated into heat losses that were not caused by the generated heat power in the resistor. The cooling power was therefore estimated by the measured voltage on the resistance:

$$\dot{Q}_C = \frac{U^2}{R} \tag{7}$$

where U and R are the measured voltage and resistance, respectively.

The mechanical power $\dot{W}_m$ of the rubber tubes was determined by the average over one period of the mechanical power:

$$\dot{W}_m = f \int_0^{1/f} F(t) v(t) dt \tag{8}$$

where F and v are the measured force and the speed of the main actuator, respectively.

The COP for the refrigeration was determined by:

$$COP = \frac{\dot{Q}_C}{\dot{W}_m + \dot{W}_h} \tag{9}$$

where $\dot{W}_h$ is the loss of power due to hydraulic loss of the fluid flow in the tubes, as detailed in Appendix A. For all tested conditions, the hydraulic losses were found to be less than 6 mW.

It should be noted that the calculation of the heat flux dissipated by the hot heat exchanger was not considered for this work, as we took into account the cooling performance of the devices only, i.e. the heat taken from the cold reservoir under a given temperature span. As a consequence, under this definition, the cooling power is considered as zero when the heating source is off. The system still generated a heat flux that compensated the thermal losses. The final temperature span is therefore limited due to the intrinsic thermal losses of the

regenerator – typically proportional to the temperature span – compensated by the generated heat flux.

In order to compare both devices and plot general performance of the fabricated devices, a specific cooling power was defined as the cooling power divided by the total mass of the rubber tubes. Considering that each rubber tube behaves like an elementary heat pump moving heat from the cold zone to the hot zone, and that all tubes are connected to the same reservoirs, the total cooling power can be estimated by the sum of each tube cooling power. In other words, the cooling power was assumed to be proportional to the number of rubber tubes in parallel and so to the total mass of rubber.

5. Results

5.1 Optimal cooling conditions

Fig. 4 shows the temperature span and the cooling power of Device #2 for cyclic elongations of approximately 3.5 to 5.5 at 0.1 Hz. The ratio between the volume of moving fluid and the total fluid volume inside the regenerator's tubes was set to 1.0. This ratio is defined as V*, as found in similar works [42]. Under these operating conditions and thermally unloaded conditions (without a heat exchanger at the top), the final temperature span between the hot and cold reservoir was 10 K (Fig, 4(A)). Fig. 4(B) shows a photograph of the regenerator, and Fig. 4(C) and (D) show its temperature measured with an infrared camera. These results confirmed that the temperature along the regenerator evolved linearly with the location along the vertical axis. In the Supplementary Materials, Movie S2 shows a corresponding thermal imaging video. Under thermally loaded conditions (Fig. 4(E)), a maximum heating power very slightly below 1.5 W was obtained (140 W/kg, considering 11 g of rubber tubes), with a maximum temperature span of 8.3 K and COP > 6. Fig. 4(E) shows the variation of the temperature span between the ambient temperature and the cold reservoir: a maximum temperature span was reached when no power was applied to the heating resistor in the cold reservoir. As the heating power produced by the resistor increased, the temperature span decreased linearly. The maximum power was obtained when the temperature of the cold reservoir was reached ambient temperature. Fig. 4(F) shows the cooling power and the COP versus temperature span as well as the mechanical power of the actuator. The linear relationship between the cooling power (and, consequently, the COP) and the temperature span is evident, where the cooling power and COP are linearly decreasing with the increasing of the temperature span. This behavior is typical for active regenerative cooling systems [14,17].

For the same operating conditions (cyclic elongation factors of approximately 3.5 to 5.5 at 0.1 Hz with a V* of 1.0), Device #1 exhibited a smaller temperature span (3.8 K), a maximum cooling power of 1.2 W (230 W/kg, considering 5 g of rubber tubes), and a maximum COP of approximately 5 as compared to Device #2.

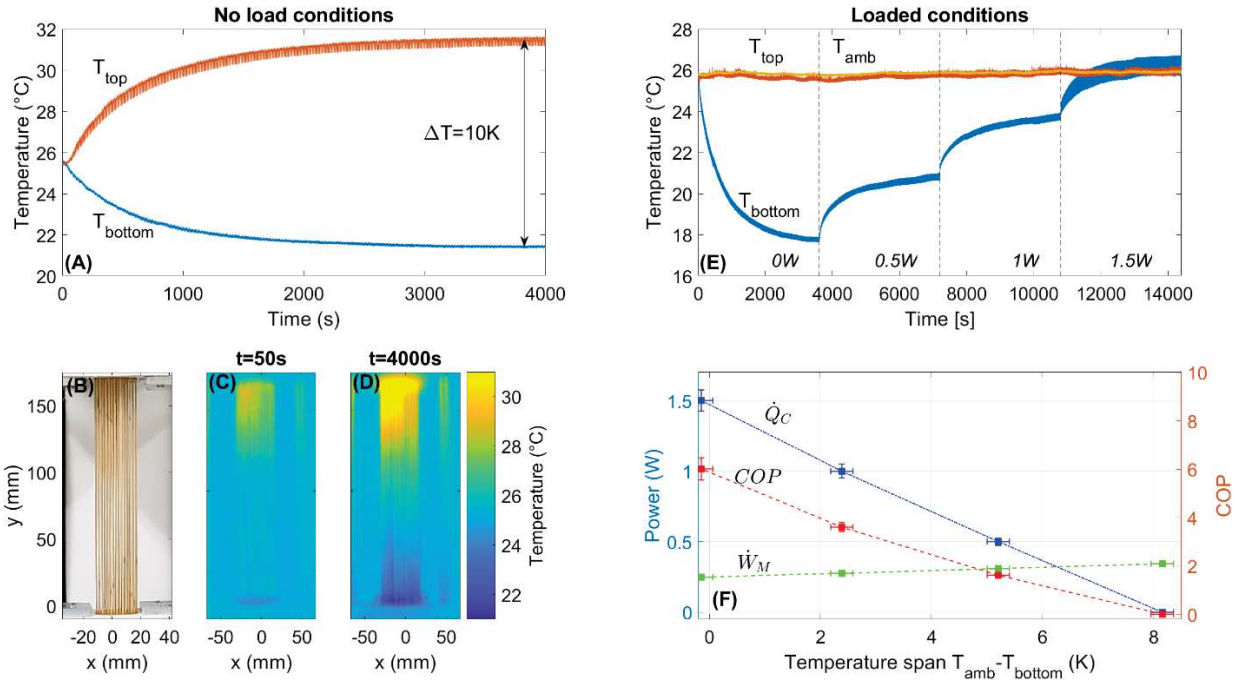

Fig. 4. Elastocaloric rubber cooler performances Device #2. (A) Measurement of the temperature span under unloaded conditions with insulated reservoirs. **(B)** Photograph of the regenerator with **(C)** its corresponding surface temperature after 50 s and **(D)** after 4000 s. **(E)** Temperature span under loaded conditions: the temperature of the top reservoir T_{top} (represented by the red curve) was maintained at approximately room temperature T_{amb} (represented by the yellow curve), whereas the temperature at the bottom reservoir T_{bottom}, (represented by the blue curve) included the heating source. At 3800, 7500, and 11000 s, the heating power was modified as indicated in italics. **(F)** Change of the cooling power ($\dot{Q}_C$), mechanical loss (W_M), and COP of Device #2 with the temperature.

5.2 Full experimental characterization

The results displayed in Fig. 4 represent the optimal operating conditions (in terms of frequency and V*) to balance the tradeoff among the temperature span, the cooling power, and the COP. To investigate the performances of the devices, we subjected them to different operating conditions. To study the influence of the fluid volume inside the regenerators, we varied the amplitude of the fluid displacement; hence, we modified the ratio between the volume of moving fluid and the total fluid volume inside the regenerator's tubes (V*). We considered four different values of V* (i.e., 0.5, 1, 1.5, and 2). We fixed the operating frequency at 0.1 Hz. Thermally loaded conditions were applied for each value of V* by varying the imposed current on the heating resistor (placed at the bottom reservoir) while keeping the top reservoir at ambient temperature. The variation of the temperature span between the bottom and the top reservoir was measured throughout the characterization and the cooling power at each imposed current was determined.

For Device #2, Fig. S1 of the Supplementary Materials shows the time variation of the measured temperature spans at different applied powers. We observed that lower values of V* led to higher temperature spans: the largest temperature span between the cold and the hot side was measured to be 9 K for V* = 0.5. However, more time was needed to reach cyclic steady-state conditions, since a smaller volume of heat transfer fluid was used to transport the heat. In contrast, the largest values of cooling power were observed for higher values of V*: a

maximum cooling power of 1.95 W (180 $W \cdot Kg^{-1}$) was achieved for V* = 2. For Device #1, Fig. S3 of the Supplementary Materials shows the time variation of the measured temperature spans at different applied powers. The same behavior was observed for Device #2: lower values of V* led to higher temperature spans (a maximum temperature span of 3.7 K was reached for V* = 0.5) and higher values of V* led to higher cooling powers (a maximum cooling power of 1.8 W (360 $W \cdot Kg^{-1}$) was reached for V* = 2).

Next, to investigate the influence of the operating frequency, we repeated the same characterization (i.e., the investigation of the variation of the fluid volume with thermally loaded conditions), fixing the frequency of the cyclic elongations at 0.2 Hz. Fig. S2 of the Supplementary Materials shows the time variation of the measured temperature spans at different applied powers when fixing the frequency at 0.2 Hz. Although the temperature span was lower compared to the case at 0.1 Hz, higher values of the cooling power were reached due to increased cycling of the elastocaloric material over time. A maximum value of 3.5 W (318 $W \cdot Kg^{-1}$) was achieved for V* = 2. For Device #1, Fig. S4 of the Supplementary Materials shows the time variation of the measured temperature spans under loaded conditions at different applied powers. Similar to what was observed for Device #2, a higher operating frequency led to higher values of the cooling power: 2 W (400 $W \cdot Kg^{-1}$) was achieved for V* = 2.

Curves of the cooler characteristics were then obtained by plotting the cooling powers and the resulting COP against the temperature spans:

- For Device #2, Fig. 5(A) and Fig. 5(B) show the cooler characteristic curves at 0.1 Hz, whereas Fig. 5(C) and Fig. 5(D) show the cooler characteristic curves at 0.2 Hz. The error bars show the ranges given by the uncertainty in the cooling power and temperature measurements. The linear behavior between the temperature span and the cooling power (and the COP) was confirmed. Moreover, the slope of the curve increases as the operating frequency and V* increase. The COP was calculated following the procedure given in Section 4.3. At 0.1 Hz, a maximum COP of 7 was reached for V* = 2, whereas at 0.2 Hz a maximum COP of 9.7 was recorded for both V* = 1.5 and V* = 2.
- For Device #1, Fig. 6 shows the resulting plots of the cooling power vs. temperature span at 0.1 Hz (Fig. 6(A)) and 0.2 Hz (Fig. 6(C)) and the plots of COP vs. temperature span at 0.1 Hz (Fig. 6(B)) and 0.2 Hz (Fig. 6(D). Compared to Device #2, higher values of COP were found, leading to a maximum COP of 12 at 0.1 Hz (Fig 6(B)) and 13 at 0.2 Hz (Fig. 6(C)). The increase in COP was mainly caused by the application of lower force levels and by a more efficient use of the active material, since Device #1 has the same wall thickness as Device #2 but double the internal diameter.

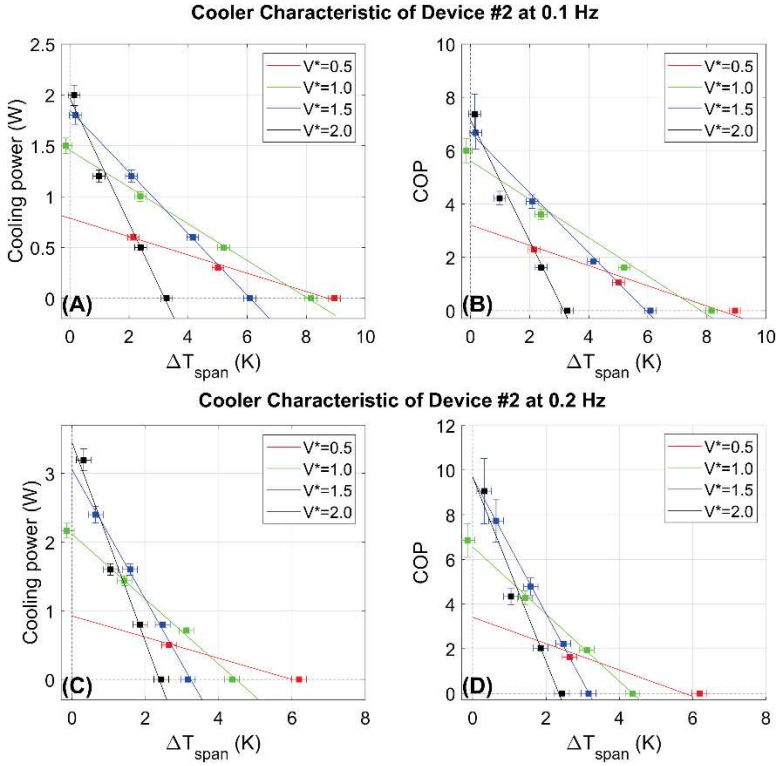

Fig. 5. Cooler characteristics (Cooling power vs. ΔT_{span} and COP vs. ΔT_{span}) of Device #2 under various operating conditions. (A) Cooling power vs. temperature span at 0.1 Hz for different values of V*. **(B)** COP vs. temperature span at 0.1 Hz for different values of V*. **(C)** Cooling power vs. temperature span at 0.2 Hz for different values of V*. **(D)** COP vs. temperature span at 0.1 Hz for different values of V*.

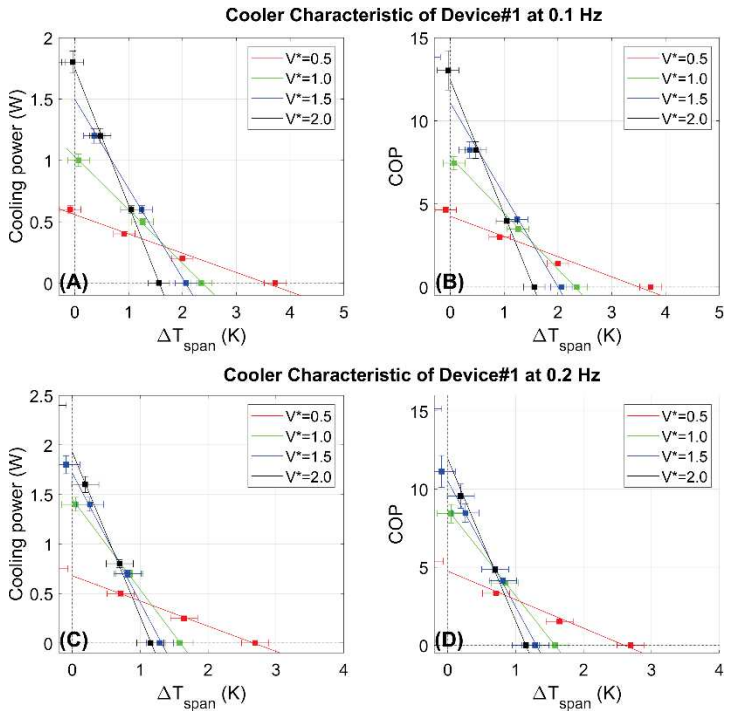

Fig. 6. Cooler characteristics (Cooling power vs. ΔT_{span} and COP vs. ΔT_{span}) of Device #1 under various operating conditions. (A) Cooling power vs. temperature span at 0.1 Hz for different values of V*. **(B)** COP vs. temperature span at 0.1 Hz for different values of V*. **(C)** Cooling power vs. temperature span at 0.2 Hz for different values of V*. **(D)** COP vs. temperature span at 0.1 Hz for different values of V*.

A summary of the performance results for Device #1 and Device #2 is shown in Fig. 7, which presents plots of the maximum values of the temperature span, cooling power, and COP obtained for the 16 different operating conditions (variations of frequency and V*) to which both devices were subjected. We observed the followings:

- for Device #2, on the one hand, higher frequencies and V* values generated a higher cooling power (3.5 W at 0.1 Hz at a V* of 2.0 in Fig. 7(B)) and COP (approximately 10 at 0.1 Hz at a V* of 2.0 in Fig. 7(C)), but a lower temperature span (2.4 K). On the other hand, lower frequencies and V* values generated higher temperature spans (~9 K at 0.1 Hz at a V* of 0.5 in Fig. 7(A)) but a lower cooling power (0.8 W at 0.1 Hz at a V* of 0.5 in Fig. 7(B));
- For Device #1, the levels of the cooling power (Fig. 7(E)) and temperature span (Fig. 7(D)) were lower than those of Device #2. Moreover, Device #1 was less sensitive to frequency change compared to Device #2, for which different frequencies lead to very different values of the cooling power and COP. The trends for each device, along with the difference in the results between the two devices, confirmed the positive impact of the geometry, particularly of the NR tubes' diameter;
- Overall, for both devices, no optimal value of V* that would maximize either the temperature span or the cooling power was found, probably due to the low passive thermal conductivity of NR. More details concerning this matter are given in Section 6.

Table 2 summarizes the results of both devices obtained from all operating conditions at all tested cooling powers, allowing comparison among the obtained values of temperature span, cooling power, and COP based on the change of frequency, V*, and the applied power on the heating resistor. We highlighted the values representing the optimization of both the temperature span and the cooling power at 0.1 Hz (yellow highlighted text), and at 0.2 Hz (green highlighted text). For both cases, we considered the optimal operating conditions to correspond to the results obtained at non-zero conditions for both the power and the temperature span.

We determined the efficiencies of the devices as the ratio of the obtained COP and the Carnot COP using the following relation:

$$\eta = \frac{COP}{COP_{Carnot}} = COP\frac{\Delta T_{span}}{T_{cold}} \tag{10}$$

where ΔT_{span} and T_{cold} represent the temperature difference between hot and cold reservoirs, and the cold reservoir temperature respectively. Using the values of Table 2 for each working condition, this yielded an efficiency of a few percent (3.3% for Device #2 for V* = 1 at 0.1 Hz and 1.8% for Device #1 for V* = 1.5 at 0.1 Hz), which is limited mostly by the temperature spans of the devices. Doubling the temperature span (e.g., by changing the geometry or the diameter of the tubes, and with a better control of the thermal losses) would double the efficiency of the regenerators.

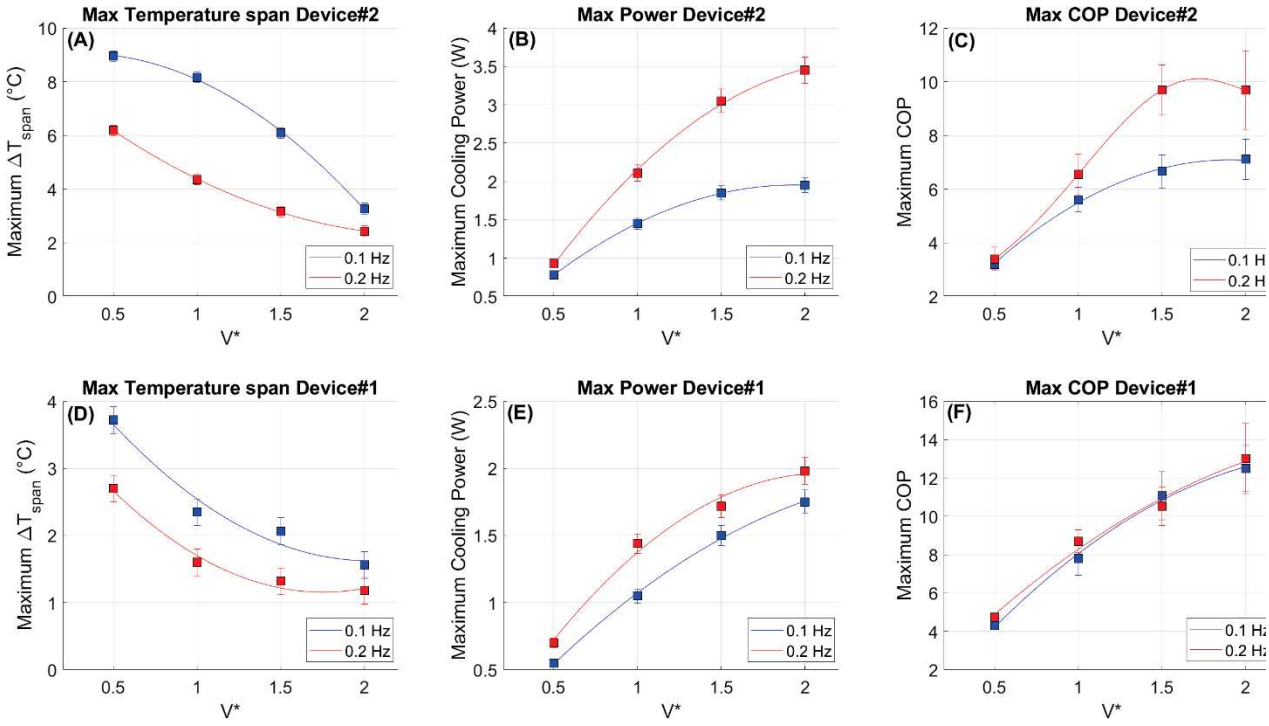

Fig. 7. Summary of the overall performances of the fabricated devices. (A) Maximum values of temperature span vs. V*, **(B)** maximum values of cooling power vs. V*, and **(C)** maximum COP vs. V* of Device #2 at 0.1 and 0.2 Hz. **(D)** Maximum temperature span vs. V*, **(E)** maximum values of cooling power vs. V*, and **(F)** maximum values of COP vs. V* of Device #1 at 0.1 and 0.2 Hz.

ΔT_{span} (K) for Device #1

V* / f (Hz)	0.5	1	1.5	2
0.1	3.7 2.0 0.9 -0.1	2.4 1.3 0.1	2.1 1.2 0.4	1.6 1.1 0.5 0
0.2	2.7 1.7 0.7 -0.2	1.6 0.9 0.1	1.3 0.8 0.3 -0.1	1.2 0.7 0.2 -0.3

ΔT_{span} (K) for Device #2

V* / f (Hz)	0.5	1	1.5	2
0.1	9.0 5.0 2.2 -1.1	8.2 5.2 2.4 -0.1	6.1 4.2 2.1 0.2	3.3 2.4 1.0 0.1
0.2	6.2 2.7 -0.9	4.4 3.1 1.4 -0.1	3.2 2.5 1.6 0.7	2.4 1.9 1.1 0.3

$\dot{Q}_C$ (W) for Device #1

V* / f (Hz)	0.5	1	1.5	2
0.1	0 0.2 0.4 0.6	0 0.5 1.1	0 0.6 1.2 1.5	0 0.6 1.2 1.8
0.2	0 0.3 0.5 0.8	0 0.7 1.4	0 0.7 1.4 1.7	0 0.8 1.6 2.0

$\dot{Q}_C$ (W) for Device #2

V* / f (Hz)	0.5	1	1.5	2
0.1	0 0.3 0.6 0.8	0 0.5 1.0 1.5	0 0.6 1.2 1.9	0 0.5 1.2 2.0
0.2	0 0.51 0.93	0 0.7 1.4 2.2	0 0.8 1.6 3.1	0 0.8 1.6 3.4

COP for Device #1

V* / f (Hz)	0.5	1	1.5	2
0.1	0 1.4 3.0 4.3	0 3.5 7.8	0 4.2 8.3 11.1	0 4.0 8.2 12.5
0.2	0 1.5 3.3 4.7	0 4.0 8.7	0 4.1 8.5 10.5	0 4.8 9.6 12

COP for Device #2

V* / f (Hz)	0.5	1	1.5	2
0.1	0 1.1 2.3 3.2	0 1.6 3.6 6.0	0 1.9 4.1 6.7	0 1.6 4.2 7.4
0.2	0 1.6 3.5	0 1.9 4.3 6.8	0 2.2 4.7 9.7	0 2.0 4.3 9.7

Table 2. Complete list of characteristics of the coolers. Summary of the obtained values of temperature span ΔTs_{pan}, cooling power $\dot{Q}_C$, and COP for Device #1 and Device #2 based on the change of frequency, V*, and the applied power on the heating resistor. The highlighted values represent the optimal operating conditions for optimizing both the temperature span and the cooling power at 0.1 Hz (yellow highlighted text) and 0.2 Hz (green highlighted text).

6. Discussion

We have presented experimental elastocaloric polymer coolers with two different geometries, wherein NR tubes were selected as an elastocaloric material. Because NR is a material with low thermal conductivity, the impact of its geometry and the operating conditions on the cooler characteristics were presumed to be potentially different from the impact of other caloric materials. Therefore, tubes with two different diameters were fabricated and tested. The tubes were first subjected to adiabatic and cyclic elongations to examine the elastocaloric properties of the NR tubes. Cycling elongations between $\lambda = 3.5$ and $\lambda = 5.5$ were found to be an appropriate compromise between the temperature variations and mechanical losses, with an adiabatic temperature variation ranging from 3.3 K to 3.7 K and mechanical losses limited to 0.27 $MJ \cdot m^{-3}$.

All-polymer cooling devices were then designed, fabricated, and tested. We used two different geometries to investigate the impact of the fluid channel diameter on the regenerator

performance: Device #1 consisted of 19 parallel tubes, each one with an inner diameter of 3.2 mm, and Device #2 consisted of 55 parallel tubes, each one with an inner diameter of 1.6 mm. The performance of each device was characterized under varied operating conditions, depending on the values of the applied frequency and the fluid displacement. Higher frequencies and higher values of fluid displacement generated a higher cooling power and COP but a smaller temperature span.

The difference in the performance between Device #1 and Device #2 was due mainly to the difference in the inner diameters of the two devices. This difference had a particularly strong impact on the regeneration factor, defined as the ratio of the temperature span of the system, ΔT_{span}, and the adiabatic temperature change of the caloric material, ΔT_{ad} [42]. For V* = 1 and f = 0.1 Hz, the regeneration factors were 1.08 and 2.44 for Device #1 and Device #2, respectively, in relation to the increase of the effective heat exchange coefficient between the heat transfer fluid and the active material. For Device #2, the effective heat transfer coefficient was ~1500 W/(m²·K) (see Appendix B for the determination of the effective heat transfer coefficient). Following the correlation suggested in [42], this calculation would lead to a regenerator factor of approximately 0.9 instead of the experimental result of 2.4, probably thanks to the low passive thermal conduction of NR, thus minimizing longitudinal heat loss and favoring the thermal gradient. The effective heat exchange coefficient—and the temperature span—could be further increased by decreasing the inner diameter of the rubber tubes, if the thermal boundary layer of the fluid spans the entire fluid channel [41]. The gain from Device #1 to Device #2 confirms this tendency. Another key point to be addressed for improving the system is the wall thickness of the rubber tubes. Decreasing this parameter would increase the regeneration factor due to both an increase of the heat transfer coefficient between the rubber and the water and a reduction of the ratio between the active material and the water, thus increasing the final cooling power. A more efficient heat exchange between the rubber and the water due to the reduction of the tube's thickness can be explained by the associated thermal resistance, which was directly proportional to the material thickness and inversely proportional to the thermal conductivity. In other words, a lower wall thickness translated to a more efficient use of the total volume of the active material.

The evolution of the temperature span and the cooling power for large V* is comparable to those of other prototypes using metallic compounds [43] and parallel plate systems [10,17,44]. However, a decrease in V* usually led to a peak for the temperature span [17,44], which was not found in our experiments. Among several interpretations, the most plausible was the impact of the low passive thermal conductivity of NR, which was found to be beneficial, as it decreased the thermal losses based on the length of the regenerator for low V* values. The relatively low thermal conductivity of rubber thus provides new optimal solutions to be explored in the future.

The control of thermal losses could be optimized thanks to a bigger size of the system. This is, however, not applicable for active thermal losses, which are intrinsic and would not be optimized from any scale effect. As discussed above, only a change of the geometry could mitigate the intrinsic thermal losses, by increasing the area of the interface between the rubber and the fluid for a given volume of fluid.

The fatigue lives of the NR tubes were not determined in this work, which instead focused on the design and testing of the cooling devices. Nevertheless, the entire characterization of each device represented several days of continuous work, reaching up to 3×10^4 cycles for each device. No significant degradation of the rubber tubes and no decrease of the elastocaloric activity were observed. In further work, the fatigue life would necessitate a dedicated

investigation, driven by the promising data from the literature; e.g., in one study, 1.7×10^5 cycles were successfully applied to NR films without any failure or decrease in the elastocaloric activity [26]. In another study, by Cadwell et al. [45], the dynamic fatigue life of NR filled with carbon black was proven to be up to 10^7 cycles under similar loading conditions; this latter value would represent more than three years of continuous operation at 0.1 Hz if it were confirmed for these elastocaloric NR tubes. Okui *et al* [46] confirmed the possibility of extending the fatigue life of elastomer by taking advantage of strain induced crystallization of NR. The type and the density of crosslink also plays an important role towards the improvement of fatigue life: Mars *et al.* mentioned that NR crosslinked with polysulfidic crosslink have a longer fatigue life than NR having monosulfidic or carbon-carbon crosslinks, it opens perspectives to optimize the formulation [47].

How does NR, a low-thermal conductivity material, compare to other caloric materials? Fig. 8(A) compares the representative device performances with the most competitive, state-of-the-art, scalable regenerative cooling systems as a function of the specific cooling power and temperature span. This comparison includes only devices for which a possible pathway is indicated for the parallelization of several active materials using a stacked active material and an oscillating fluid flow or using a multi-stage system and for which the power or the temperature span or both can be increased with the number of active materials. Elastocaloric rubber, studied in this work, falls in the upper range for the cooling power (with the exception for the latest results from Ahcin *et al.* [21]), thus demonstrating the competitiveness of NR—a low-thermal-conductivity material—for scalable regenerative cooling devices. Fig. 8(B) compares the absolute values of power obtained with the devices developed in this work with both regenerative and non-regenerative systems (*i.e.*, systems not coupled with an oscillating fluid flow) that use polymer or ceramic materials, which exhibit low thermal conductivities. The results of our work led to the highest absolute value of the cooling power for polymer and ceramic-based devices, including both elastocaloric and electrocaloric materials.

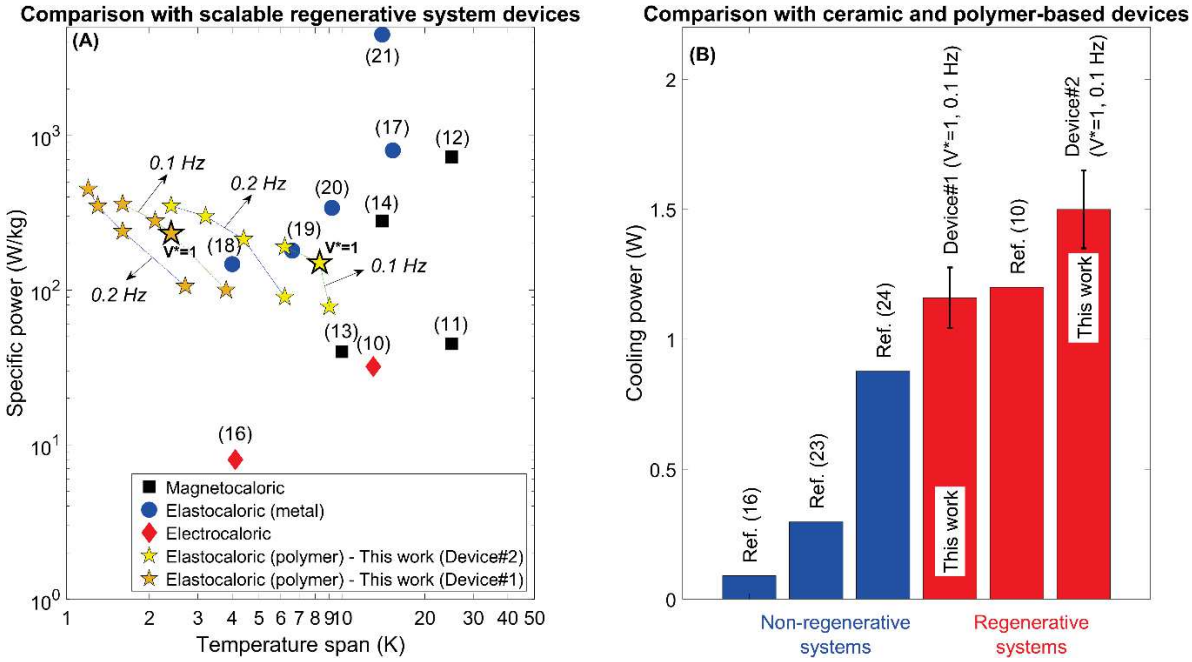

Fig. 8. Comparison with other caloric material cooling systems from the literature. (A) Specific power vs. temperature span of scalable regenerative caloric cooling systems. **(B)** Maximum achieved cooling power for ceramic- and polymer-based coolers and heat pumps.

7. Conclusion

In this work, two all-polymer cooling devices (Device #1 and Device #2) were designed, fabricated, and tested. The influence of the frequency and the volume of heat transfer fluid were found to be non-trivial parameters influencing the final temperature span and cooling power of the systems. We found a frequency of 0.1 Hz and a V* value of 1.0 as the optimal operating conditions for Device #2. Under these operating conditions, a maximum heating power of 1.5 W (140 W/kg) was obtained, with a temperature span of 8.3 K and COP > 6. For the same operating conditions, Device #1 exhibited a smaller temperature span (3.8 K), a cooling power of 1.2 W (230 W/kg), and COP ~ 5. Thus, the reduction of the diameter of the tubes by a factor of two increased the temperature span by a factor of two, while keeping a large specific cooling power. A further reduction of the tubes' diameter is expected to improve the performance similarly. The low thermal conductivity of NR did not lead to any problem with heat exchange, thanks to the adequate wall thickness of rubber compared to the thickness of the harmonic thermal boundary layer. In contrast, the low thermal conductivity did provide an advantage in the thermal gradient of the regenerators, leading to a larger regeneration factor than was suggested by the tendency established from literature. Moreover, the temperature span and cooling power were found to exhibit a monotonic dependence on the displaced fluid volume, contrary to the case of metallic caloric materials, for which an optimum is usually found.

We thus confirmed that a proper design and implementation allowed the use of numerous tubes in parallel, all working with pre-elongated states. The two prototypes presented in this article suggest the potential of the application of NR for refrigeration and are not intended to constitute a full-scale prototype. The cooling power remained in the watt range (up to 3.5 W) with 55 parallel tubes. The proposed polymer-based cooling devices demonstrated the high potential of NR for scalable regenerative cooling devices, with performances as high as that of other caloric materials presented along with these prototypes. Although the prototypes represent experimental proof-of-concepts at a laboratory scale, the successful parallelization of rubber tubes is foreseen to pave the way towards realistic elastocaloric polymer heat pumps and cooling devices on larger scale attempts, as the number of tubes may be further increased with the same general structure and fabrication technique. This would immediately lead to an increase of the cooling power. The further optimization of the geometry of the system and the formulation of the material could also enhance the COP and temperature span. Finally, the significant advantages of using NR are its low cost and abundance, as well as the existence of various potential recycling solutions [48] for reusing NR in blends, including as elastocaloric materials [49], thus contributing to make this alternative refrigeration system sustainable. Research on elastocaloric polymers remains in its early stages; further investigation on NR refrigeration as well a further materials and systems improvements could probably lead to higher performances.

Acknowledgment

This work was performed within the framework of the International Research Network ELyT Global. The work was financially supported by the following fundings: Agence Nationale pour la Recherche (ANR, France) ANR-17-CE05-0016, Japan Society for the Promotion of Science (JSPS, Japan) Grant-in-Aid for Scientific Research 19K04230.

Competing Interest Statement

GS and AK have filed a patent application related to the main technical parts of the regenerator fabrication (EP22160602). The other authors declare no competing interests.

Appendix A

The hydraulic connections of the different tubes involve collecting chambers and variations in the rubber tube diameters near the heat exchangers. Therefore, the hydraulic losses were not calculated theoretically by the friction loss of the fluid circulation into the tubes. The hydraulic losses were determined by measuring the time required to empty a 10 mL reservoir placed above the top reservoir using gravity only.

For Device #1 and Device #2, the time required was 0.5 and 7.1 s, respectively. The fluid displacement was attributed to a constant static pressure:

$$p = \rho_f GL, \tag{A.1}$$

where L is the total height of the regenerator, G is the constant of gravity, and ρ_f is the density of the fluid.

The hydraulic losses were presumed to be proportional to the volumetric flow rate $p = \alpha \dot{V}$, where $\dot{V}$ was estimated to be the total volume of 10 mL divided by the time of fluid motion t_0. The hydraulic loss coefficient is therefore given by:

$$\alpha = t_0 \frac{\rho_f GL}{V_{tot}}, \tag{A.2}$$

where V_{tot} is the total volume of the reservoir, and t_0 is the time to empty the reservoir.

The hydraulic losses during the operation of the elastocaloric system were calculated by using the effective flow rate and frequency. During operation, the fluid was moved twice per period during a time t_1, each time at a constant velocity:

$$\dot{V}_r = \frac{V^* V_{REG}}{t_1}, \tag{A.3}$$

where V^* is the ratio between the volume of fluid and the total volume inside the regenerator's tubes, and V_{REG} is the volume of the regenerator.

The average hydraulic loss was then obtained by:

$$\dot{W}_h = 2t_1 f p \dot{V}_r = 2t_1 f \alpha \dot{V}_r^2 = 2t_1 f t_0 \frac{\rho_f GL}{V_{tot}} \left(\frac{V^* V_{REG}}{t_1}\right)^2 \tag{A.4}$$

For Device #1 at 0.2 Hz, $\dot{W}_h$ ranged from 0.03 mW (for V* = 0.5) to 0.5 mW (for V* = 2). For Device #2 at 0.2 Hz, $\dot{W}_h$ ranged from 0.4 mW (for V* = 0.5) to 6 mW (for V* = 2). In both cases, the hydraulic losses were found to be negligible compared with the measured cooling power in the watts range. For future work, the calculation of the pressure drop could be improved by installing pressure sensors at each side of the regenerators (similar to the work of Qian et al. [50]).

Appendix B

To analyze the difference between the two geometries, the effective exchange heat transfer coefficient between the rubber tube and fluid was calculated in both cases. Following the analysis provided in [42,51], the effective heat exchange coefficient h_{eff} is given by:

$$h_{eff} = \frac{h}{1 + \frac{Bi}{a_0}}, \tag{B.1}$$

where h is the uncorrected heat transfer coefficient, related to the geometry and properties of the

fluid only; Bi is the Biot number, related to the limits induced by the thermal conductivity and the geometry of the solid; and a_0 is a geometric factor, equal to 4 for cylindrical tubes.

The Biot number is given by

$$Bi = \frac{R_{TH\_conduction}}{R_{TH\_convection}} \tag{B.2}$$

where $R_{TH\_conduction}$ and $R_{TH\_convection}$ are the thermal resistances within the solid wall and at the interface between the solid and the fluid, respectively. They are given by:

$$R_{TH_{conduction}} = \frac{1}{K2\pi} \ln\left(\frac{d_{ext}}{d_{int}}\right) \tag{B.3}$$

$$R_{TH\_convection} = \frac{1}{h\pi d_{int}} \tag{B.4}$$

where d_{ext} and d_{int} are the external and internal diameters, respectively, of the stretched rubber tubes, and K is the thermal conductivity of the rubber material.

The Reynolds number is small in the studied system: Re<20 for all tested conditions of the geometry and the volumetric flow rate. Therefore, the Nusselt number was taken at a fixed value of 3.66 for a fully developed laminar flow inside the cylindrical tubes with a constant wall temperature (neglecting entry effects [37] since the length to diameter ratio exceeds 100). Consequently, the heat transfer coefficient is given by:

$$h = \frac{Nu\, k_f}{d_{int}}. \tag{B.5}$$

Therefore, the effective heat transfer coefficient depends on the geometry of the regenerator only, independently of the fluid flow rate. Raw heat transfer coefficients of approximately 1500 and 3000 W/(m²·K) were found for Device #1 and Device #2, respectively. Effective heat transfer coefficients of ~900 and ~1500 W/(m²·K) were found for Device #1 and Device #2, respectively. Based on a general correlation proposed in [42], these values suggest a regeneration factor of 0.5 for Device #1 and 0.9 for Device #2, which were much lower in both devices than what was observed in the experiments.

References

[1] IEA (2021), Cooling, IEA, Paris https://www.iea.org/reports/cooling. n.d.

[2] ASHRAE. ASHRAE. 15 & 34 Safety Standard for Refrigeration Systems and Designation and Classification of Refrigerants ISO 5149 Mechanical Refrigerating Systems Used for Cooling and Heating—Safety Requirements. Available online: https://www.ashrae.org/technical-res. 2018. https://doi.org/https://www.ashrae.org/technical-resources/bookstore/standards-15-34.

[3] Kim MH, Pettersen J, Bullard CW. Fundamental process and system design issues in CO2 vapor compression systems. vol. 30. 2004. https://doi.org/10.1016/j.pecs.2003.09.002.

[4] Baek C, Heo J, Jung J, Cho H, Kim Y. Optimal control of the gas-cooler pressure of a CO2 heat pump using EEV opening and outdoor fan speed in the cooling mode. Int J Refrig 2013;36:1276–84. https://doi.org/10.1016/j.ijrefrig.2013.02.009.

[5] Yang D, Song Y, Cao F, Jin L, Wang X. Theoretical and experimental investigation of a combined R134a and transcritical CO2 heat pump for space heating. Int J Refrig 2016;72:156–70. https://doi.org/10.1016/j.ijrefrig.2016.07.016.

[6] Aprea C, Greco A, Maiorino A, Masselli C. The environmental impact of solid-state materials working in an active caloric refrigerator compared to a vapor compression cooler. Int J Heat Technol 2018;36:1155–62. https://doi.org/10.18280/ijht.360401.

[7] Calm JM. The next generation of refrigerants - Historical review, considerations, and outlook. Int J Refrig 2008;31:1123–33. https://doi.org/10.1016/j.ijrefrig.2008.01.013.

[8] Greco A, Aprea C, Maiorino A, Masselli C. A review of the state of the art of solid-state caloric cooling processes at room-temperature before 2019. Int J Refrig 2019;106:66–88. https://doi.org/10.1016/j.ijrefrig.2019.06.034.

[9] Ossmer H, Wendler F, Gueltig M, Lambrecht F, Miyazaki S, Kohl M. Energy-efficient miniature-scale heat pumping based on shape memory alloys. Smart Mater Struct 2016;25. https://doi.org/10.1088/0964-1726/25/8/085037.

[10] Torelló A, Lheritier P, Usui T, Nouchokgwe Y, Gérard M, Bouton O, et al. Giant temperature span in electrocaloric regenerator. Science (80-) 2020;370. https://doi.org/10.1126/science.abb8045.

[11] Hirano N. Development of magnetic refrigerator for room temperature application, AIP Publishing; 2003, p. 1027–34. https://doi.org/10.1063/1.1472125.

[12] Tura A, Rowe A. Permanent magnet magnetic refrigerator design and experimental characterization. Int J Refrig 2011;34:628–39. https://doi.org/10.1016/j.ijrefrig.2010.12.009.

[13] Tušek J, Kitanovski A, Tomc U, Favero C, Poredoš A. Experimental comparison of multi-layered La-Fe-Co-Si and single-layered Gd active magnetic regenerators for use in a room-temperature magnetic refrigerator. Int. J. Refrig., vol. 37, 2014, p. 117–26. https://doi.org/10.1016/j.ijrefrig.2013.09.003.

[14] Bahl CRH, Engelbrecht K, Eriksen D, Lozano JA, Bjørk R, Geyti J, et al. Development and experimental results from a 1 kW prototype AMR. Int J Refrig 2014;37:78–83. https://doi.org/10.1016/j.ijrefrig.2013.09.001.

[15] Lionte S, Risser M, Muller C. A 15kW magnetocaloric proof-of-concept unit: Initial development and first experimental results. Int J Refrig 2021;122:256–65. https://doi.org/10.1016/j.ijrefrig.2020.09.019.

[16] Wang Y, Zhang Z, Usui T, Benedict M, Hirose S, Lee J, et al. A high-performance solid-state electrocaloric cooling system. Science (80-) 2020;370:129–33. https://doi.org/10.1126/science.aba2648.

[17] Tušek J, Engelbrecht K, Eriksen D, Dall'Olio S, Tušek J, Pryds N. A regenerative elastocaloric heat pump. Nat Energy 2016;1. https://doi.org/10.1038/nenergy.2016.134.

[18] Qian S, Wang Y, Geng Y, Ling J, Muehlbauer J, Suxin Qian A, et al. International Refrigeration and Air Conditioning Conference. Paper 1726. 16 th International Refrigeration and Air Conditioning Conference at Purdue. 2016.

[19] Snodgrass R, Erickson D. A multistage elastocaloric refrigerator and heat pump with 28 K temperature span. Sci Rep 2019;9. https://doi.org/10.1038/s41598-019-54411-8.

[20] Chen Y, Wang Y, Sun W, Qian S, Liu J. A compact elastocaloric refrigerator. Innov 2022;3. https://doi.org/10.1016/j.xinn.2022.100205.

[21] Ahčin Ž, Dall'Olio S, Žerovnik A, Baškovič UŽ, Porenta L, Kabirifar P, et al. High-performance cooling and heat pumping based on fatigue-resistant elastocaloric effect in compression. Joule 2022;6:2338–57. https://doi.org/10.1016/j.joule.2022.08.011.

[22] Wang R, Fang S, Xiao Y, Gao E, Jiang N, Li Y, et al. Torsional refrigeration by twisted, coiled, and supercoiled fibers. Science (80-) 2019;366:216–21.

https://doi.org/10.1126/science.aax6182.

[23] Ma R, Zhang Z, Tong K, Huber D, Kornbluh R, Ju YS, et al. Highly efficient electrocaloric cooling with electrostatic actuation. Science (80-) 2017;357:1130–4. https://doi.org/10.1126/science.aan5980.

[24] Greibich F, Schwödiauer R, Mao G, Wirthl D, Drack M, Baumgartner R, et al. Elastocaloric heat pump with specific cooling power of 20.9 W g–1 exploiting snap-through instability and strain-induced crystallization. Nat Energy 2021;6:260–7. https://doi.org/10.1038/s41560-020-00770-w.

[25] Xie Z, Sebald G, Guyomar D. Elastocaloric effect dependence on pre-elongation in natural rubber. Appl Phys Lett 2015;107. https://doi.org/10.1063/1.4929395.

[26] Sebald G, Xie Z, Guyomar D. Fatigue effect of elastocaloric properties in natural rubber. Philos Trans R Soc A Math Phys Eng Sci 2016;374. https://doi.org/10.1098/rsta.2015.0302.

[27] Ruellan B, Le Cam JB, Jeanneau I, Canévet F, Mortier F, Robin E. Fatigue of natural rubber under different temperatures. Int J Fatigue 2019;124:544–57. https://doi.org/10.1016/j.ijfatigue.2018.10.009.

[28] Imran M, Zhang X. Recent developments on the cyclic stability in elastocaloric materials. Mater Des 2020;195. https://doi.org/10.1016/j.matdes.2020.109030.

[29] Sebald G, Komiya A, Jay J, Coativy G, Lebrun L. Regenerative cooling using elastocaloric rubber: Analytical model and experiments. J Appl Phys 2020;127. https://doi.org/10.1063/1.5132361.

[30] Mitchell JC, Meier DJ. Rapid stress- induced crystallization in natural rubber. J Polym Sci Part A- 2 Polym Phys 1968;6(10):1689–703. https://doi.org/https://doi.org/10.1002/pol.1968.160061001.

[31] J. Pellicer, J. A. Manzanares, J. Zúñiga and PU. Thermodynamic of rubber elasticity. Proc R Soc London Ser A 1976;351:331–50. https://doi.org/10.1098/rspa.1976.0145.

[32] Xie Z, Wei C, Guyomar D, Sebald G. Validity of Flory's model for describing equilibrium strain-induced crystallization (SIC) and thermal behavior in natural rubber. Polymer (Guildf) 2016;103:41–5. https://doi.org/10.1016/j.polymer.2016.09.038.

[33] Dart SL, Guth E. Rise of temperature on fast stretching of butyl rubber. J Chem Phys 1945;13:28–36. https://doi.org/10.1063/1.1723964.

[34] Ichiro T, Karl S. Solid-state cooling with caloric materials. Phys Today 2015;68:48.

[35] Treloar LR. The Physics of Rubber Elasticity. Oxford Universty Press; 1975.

[36] Tosaka M, Kawakami D, Senoo K, Kohjiya S, Ikeda Y. Crystallization and stress relaxation in highly-stretched samples of natural rubber. Polym Prepr Japan 2006;55:3389–90. https://doi.org/https://doi.org/10.1021/ma060407+.

[37] Trevizoli P V., Peixer GF, Nakashima AT, Capovilla MS, Lozano JA, Barbosa JR. Influence of inlet flow maldistribution and carryover losses on the performance of thermal regenerators. Appl Therm Eng 2018;133:472–82. https://doi.org/10.1016/j.applthermaleng.2018.01.055.

[38] Sebald G, Seveyrat L, Capsal J, Cottinet P, Guyomar D. Differential scanning calorimeter and infrared imaging for electrocaloric characterization of poly (vinylidene fluoride-. Appl Phys Lett 2012;101:022907.

[39] Xie Z, Sebald G, Guyomar D. Temperature dependence of the elastocaloric effect in natural rubber. Phys Lett Sect A Gen At Solid State Phys 2017;381:2112–6. https://doi.org/10.1016/j.physleta.2017.02.014.

[40] Trabelsi S, Albouy PA, Rault J. Crystallization and melting processes in vulcanized stretched natural rubber. Macromolecules 2003;36:7624–39. https://doi.org/10.1021/ma030224c.

[41] van Buren SH, Polifke W. Enhanced Longitudinal Heat Transfer in Oscillatory Channel Flow—A Theoretical Perspective. J Fluids Eng Trans ASME 2021;143. https://doi.org/10.1115/1.4052067.

[42] Torelló, Defay E. Heat exchange law in caloric regenerators. Int J Refrig 2021;127:174–9. https://doi.org/10.1016/j.ijrefrig.2021.02.024.

[43] Trevizoli P V., Nakashima AT, Barbosa JR. Performance evaluation of an active magnetic regenerator for cooling applications – part II: Mathematical modeling and thermal losses. Int J Refrig 2016;72:206–17. https://doi.org/10.1016/j.ijrefrig.2016.07.010.

[44] Engelbrecht K, Tušek J, Eriksen D, Lei T, Lee CY, Tušek J, et al. A regenerative elastocaloric device: Experimental results. J Phys D Appl Phys 2017;50. https://doi.org/10.1088/1361-6463/aa8656.

[45] Cadwell SM, Merrill RA, Sloman CM, Yost FL. Dynamic Fatigue Life of Rubber. Rubber Chem Technol 1940;13:304–15. https://doi.org/10.5254/1.3539515.

[46] Okui M, Kojima A, Hisamichi I, Kuriyama S, Kojima T, Tsuji T, et al. Prolonging rubber fatigue life using hysteresis of strain-induced crystallization of natural rubber. Polym Test 2023;117:107800. https://doi.org/10.1016/j.polymertesting.2022.107800.

[47] Mars W V., Fatemi A. Factors that affect the fatigue life of rubber: A literature survey. Rubber Chem Technol 2004;77:391–412. https://doi.org/10.5254/1.3547831.

[48] Isayev AI. Recycling of natural and synthetic isoprene rubbers. Chem. Manuf. Appl. Nat. Rubber, Elsevier Inc.; 2014, p. 395–435. https://doi.org/10.1533/9780857096913.3.395.

[49] Candau N, Vives E, Fernández AI, Maspoch ML. Elastocaloric effect in vulcanized natural rubber and natural/wastes rubber blends. Polymer (Guildf) 2021;236. https://doi.org/10.1016/j.polymer.2021.124309.

[50] Qian S, Geng Y, Wang Y, Muehlbauer J, Ling J, Hwang Y, et al. Design of a hydraulically driven compressive elastocaloric cooling system. Sci Technol Built Environ 2016;22:500–6. https://doi.org/10.1080/23744731.2016.1171630.

[51] Engelbrecht KL, Nellis GF, Klein SA. The effect of internal temperature gradients on regenerator matrix performance. J Heat Transfer 2006;128:1060–9. https://doi.org/10.1115/1.2345428.